Pump-probe nonlinear phase dispersion spectroscopy

Francisco E. Robles,[1,*] Prathyush Samineni,[1] Jesse W. Wilson,[1] and Warren S. Warren[1,2]

[1]*Department of Chemistry, Duke University, Durham, North Carolina 27708, USA*
[2]*Departments of Radiology and Biomedical Engineering, Duke University, Durham, North Carolina 27708, USA*
[*]*francisco.robles@duke.edu*

Abstract: Pump-probe microscopy is an imaging technique that delivers molecular contrast of pigmented samples. Here, we introduce pump-probe nonlinear phase dispersion spectroscopy (PP-NLDS), a method that leverages pump-probe microscopy and spectral-domain interferometry to ascertain information from dispersive and resonant nonlinear effects. PP-NLDS extends the information content to four dimensions (phase, amplitude, wavelength, and pump-probe time-delay) that yield unique insight into a wider range of nonlinear interactions compared to conventional methods. This results in the ability to provide highly specific molecular contrast of pigmented and non-pigmented samples. A theoretical framework is described, and experimental results and simulations illustrate the potential of this method. Implications for biomedical imaging are discussed.

OCIS codes: (300.6420) Spectroscopy, nonlinear; (120.3180) Interferometry; (180.4315) Nonlinear microscopy; (170.3880) Medical and biological imaging; (190.3270) Kerr effect.

References and links

1. D. Fu, T. Ye, T. E. Matthews, B. J. Chen, G. Yurtserver, and W. S. Warren, "High-resolution in vivo imaging of blood vessels without labeling," Opt. Lett. **32**(18), 2641–2643 (2007).
2. D. Fu, T. E. Matthews, T. Ye, I. R. Piletic, and W. S. Warren, "Label-free in vivo optical imaging of microvasculature and oxygenation level," J. Biomed. Opt. **13**(4), 040503 (2008).
3. T. E. Matthews, I. R. Piletic, M. A. Selim, M. J. Simpson, and W. S. Warren, "Pump-probe imaging differentiates melanoma from melanocytic nevi," Sci. Transl. Med. **3**(71), 71ra15 (2011).
4. T. E. Matthews, J. W. Wilson, S. Degan, M. J. Simpson, J. Y. Jin, J. Y. Zhang, and W. S. Warren, "In vivo and ex vivo epi-mode pump-probe imaging of melanin and microvasculature," Biomed. Opt. Express **2**(6), 1576–1583 (2011).
5. P. Samineni, A. deCruz, T. E. Villafaña, W. S. Warren, and M. C. Fischer, "Pump-probe imaging of historical pigments used in paintings," Opt. Lett. **37**(8), 1310–1312 (2012).
6. M. C. Fischer, T. Ye, G. Yurtsever, A. Miller, M. Ciocca, W. Wagner, and W. S. Warren, "Two-photon absorption and self-phase modulation measurements with shaped femtosecond laser pulses," Opt. Lett. **30**(12), 1551–1553 (2005).
7. P. Samineni, Z. Perret, W. S. Warren, and M. C. Fischer, "Measurements of nonlinear refractive index in scattering media," Opt. Express **18**(12), 12727–12735 (2010).
8. J. W. Wilson, P. Samineni, W. S. Warren, and M. C. Fischer, "Cross-phase modulation spectral shifting: nonlinear phase contrast in a pump-probe microscope," Biomed. Opt. Express **3**(5), 854–862 (2012).
9. P. Samineni, B. Li, J. W. Wilson, W. S. Warren, and M. C. Fischer, "Cross-phase modulation imaging," Opt. Lett. **37**(5), 800–802 (2012).
10. E. O. Potma, W. P. de Boeij, and D. A. Wiersma, "Femtosecond dynamics of intracellular water probed with nonlinear optical Kerr effect microspectroscopy," Biophys. J. **80**(6), 3019–3024 (2001).
11. D. L. Marks and S. A. Boppart, "Nonlinear interferometric vibrational imaging," Phys. Rev. Lett. **92**(12), 123905 (2004).
12. P. D. Chowdary, Z. Jiang, E. J. Chaney, W. A. Benalcazar, D. L. Marks, M. Gruebele, and S. A. Boppart, "Molecular histopathology by spectrally reconstructed nonlinear interferometric vibrational imaging," Cancer Res. **70**(23), 9562–9569 (2010).
13. J. W. Wilson, P. Schlup, and R. A. Bartels, "Synthetic temporal aperture coherent molecular phase spectroscopy," Chem. Phys. Lett. **463**(4-6), 300–304 (2008).

#185319 - $15.00 USD Received 13 Feb 2013; revised 1 Apr 2013; accepted 4 Apr 2013; published 9 Apr 2013

14. J. W. Wilson, P. Schlup, and R. Bartels, "Phase measurement of coherent Raman vibrational spectroscopy with chirped spectral holography," Opt. Lett. **33**(18), 2116–2118 (2008).
15. B. E. Applegate and J. A. Izatt, "Molecular imaging of endogenous and exogenous chromophores using ground state recovery pump-probe optical coherence tomography," Opt. Express **14**(20), 9142–9155 (2006).
16. D. Jacob, R. L. Shelton, and B. E. Applegate, "Fourier domain Pump-Probe Optical Coherence Tomography imaging of melanin," Opt. Express **18**(12), 12399–12410 (2010).
17. U. Morgner, W. Drexler, F. X. Kärtner, X. D. Li, C. Pitris, E. P. Ippen, and J. G. Fujimoto, "Spectroscopic optical coherence tomography," Opt. Lett. **25**(2), 111–113 (2000).
18. F. E. Robles, C. Wilson, G. Grant, and A. Wax, "Molecular imaging true-colour spectroscopic optical coherence tomography," Nat. Photonics **5**(12), 744–747 (2011).
19. M. A. Choma, A. K. Ellerbee, C. Yang, T. L. Creazzo, and J. A. Izatt, "Spectral-domain phase microscopy," Opt. Lett. **30**(10), 1162–1164 (2005).
20. F. E. Robles and A. Wax, "Separating the scattering and absorption coefficients using the real and imaginary parts of the refractive index with low-coherence interferometry," Opt. Lett. **35**(17), 2843–2845 (2010).
21. F. E. Robles, L. L. Satterwhite, and A. Wax, "Nonlinear phase dispersion spectroscopy," Opt. Lett. **36**(23), 4665–4667 (2011).
22. D. McMorrow, W. T. Lotshaw, and G. A. Kenney-Wallace, "Femtosecond optical Kerr studies on the origin of the nonlinear responses in simple liquids," IEEE J. Quantum Electron. **24**(2), 443–454 (1988).
23. I. A. Heisler, R. R. B. Correia, T. Buckup, S. L. S. Cunha, and N. P. da Silveira, "Time-resolved optical Kerr-effect investigation on CS2/polystyrene mixtures," J. Chem. Phys. **123**(5), 054509 (2005).
24. Y. J. Chang and E. W. Castner, "Femtosecond dynamics of hydrogen-bonding solvents. Formamide and N-methylformamide in acetonitrile, DMF, and water," J. Chem. Phys. **99**(1), 113 (1993).
25. E. Tokunaga, A. Terasakiy, and T. Kobayashi, "Femtosecond phase spectroscopy by use of frequency-domain interference," J. Opt. Soc. Am. B **12**(5), 753–771 (1995).
26. R. W. Boyd, *Nonlinear Optics* (Elsevier, 2008).

1. Introduction

Recently a great deal of research has been focused on utilizing nonlinear optical interactions to provide molecular contrast in microscopy. For example, pump-probe microscopy measures the transient, excited state dynamic properties of pigmented samples resulting from interactions such as excited state absorption, ground state depletion, and stimulated emission; consequently the acquired signals exhibit unique structures that enable differentiation of many molecular species. This method has had a significant impact on both biomedical applications [1,2], particularly quantitative melanoma detection [3,4], and art conservation [5]. On the other hand, various techniques have been developed to provide contrast from non-pigmented samples by using nonlinear phase changes (e.g., self/cross phase modulation), which provide greater detail of a sample's morphology [6–9], but for the most part, lack molecular specificity. One exception is a modified pump-probe system that uses polarization effects to determine the diffusive motions of molecules based on the non-instantaneous components of the optical Kerr effect (i.e., nuclear response) [10].

Most nonlinear microscopy methods, however, acquire signals in the time domain and ignore the rich information content available from wavelength-dependent phenomena. In addition, few of these methods are able to analyze the complex form of optical fields, which can provide a better understanding of the different types of interactions that occur in a sample by separating the real and imaginary (dispersive and resonant, respectively) contributions. Interferometric methods, on the other hand, are well suited for both of these tasks. Nonlinear interferometric vibrational imaging (NIVI), for example, resolves the complex, wavelength-dependent field of an anti-Stokes wave in order to remove the non-resonant background in coherent anti-Stokes Raman scattering (CARS), and to allow linear estimation of the third order optical susceptibility, $\chi^{(3)}(\Omega)$, where Ω is the vibrational frequency [11,12]. Wilson et al. also proposed an interferometric method that utilizes a synthetic temporal aperture to ascertain information regarding impulsive stimulated Raman scattering by looking at the temporal phase [13] or the spectral phase of chirped pulses [14]. Pump-probe optical coherence tomography (PP-OCT) schemes have also been employed [15,16], however no attempts have been made to resolve the spectral information or the complex field from PPOCT signals.

#185319 - $15.00 USD Received 13 Feb 2013; revised 1 Apr 2013; accepted 4 Apr 2013; published 9 Apr 2013

Recently, a method named nonlinear phase dispersion spectroscopy (NLDS), an extension of spectroscopic OCT [17,18] and spectral-domain phase microscopy [19], has demonstrated the ability to independently assess the real and imaginary parts of the linear refractive index (RI), thus separating the scattering and absorption coefficients [20], and providing a more sensitive measure of absorption in biological samples [21]. In this work, NLDS is extended to assess a sample's nonlinear, real and imaginary, wavelength-dependent optical response to a pump beam (hereafter termed PP-NLDS). The method achieves this by adding a reference field to a conventional pump-probe setup at the same wavelength as the probe beam and leveraging the capabilities of interferometric detection in the spectral-domain. Different from PPOCT and the previous NLDS approach, both the probe and reference fields are sent through the sample, which isolates the desired nonlinear effects and provides a highly stable configuration. It is also worth noting that the nonlinear effects we seek to measure are very demanding on the experimental setup since the effects can be extremely small—for that reason, comparable interferometric schemes, such as the ones previously mentioned [11–14], have required the use of amplified pulses. With the approach proposed here, however, this is not necessary. As we will show, PP-NLDS uses the wavelength information to remove much of the undesired noise, particularly from the phase measurements. A theoretical framework is provided, and experimental results and simulations show that this method is indeed capable of measuring nonlinear intensity changes, similar to conventional pump-probe methods, as well as phase changes resulting from the instantaneous and non-instantaneous components of the optical Kerr effect (OKE).

2. Experimental system and methods

The experimental system, shown in Fig. 1, consists of a pump-probe setup combined with a Michelson interferometer in the probe arm, similar to that described in [13]. Specifically, the output of a mode-locked Ti:Sapphire laser (Tsunami, Spectra Physics, 80 MHz), with a centered wavelength of 808 nm, is split into two beams: The first beam pumps an optical parametric oscillator (Mira OPO, Coherent) that is tuned to 720 nm and serves as the pump beam. These wavelengths are chosen since they are routinely used for biological imaging with pump-probe microscopy [1–4]. The second beam from the Ti:Sapph laser is further split into two using a Michelson interferometer to provide a probe field and a reference field, separated by a constant time T = 1.25 mm/c = 4.16 ps, where c is the speed of light in vacuum. The three beams are combined using a dichroic mirror and are sent collinearly to a microscope objective (10X, 0.25 numerical aperture), which focuses the light onto the sample. Then, light is collimated, filtered to remove the pump beam, coupled into a single mode fiber (SMF), and sent to a spectrometer (HR4000, Ocean Optics) for detection. Note that while the pump beam does not interfere with the reference field and it is spectrally resolved on the spectrometer, it must be filtered out to prevent potential nonlinear interactions in the SMF. Further, the reference must precede the pump, otherwise the reference field would experience changes from long-lived exited states induced on the sample by the pump.

In conventional pump-probe experiments, the pump beam is typically modulated (turned on and off) at relatively high frequencies (e.g., 2 MHz) to enable detection of intensity changes resulting from nonlinear interactions using a lock-in-amplifier (LIA). For the present work, however, no modulation is introduced on the pump beam since a LIA is not employed. Instead, the pump is in the 'on' position when it arrives at the sample at the same time or before the probe ($\tau \geq 0$), and 'off' when the pump arrives after the probe ($\tau < -\tau_{pr}$, where τ_{pr} is the duration of the probe beam), which ensures that the observed behavior is not a result of thermal effects. This is achieved by introducing a cover glass onto the pump's path, which produces a delay of 700 fs. The 'on'/'off' time delay is fixed at $\tau \sim 0$ fs for the experimental results discussed in section 4. Both pulses have a duration (full width at half maximum, FWHM) of 140 fs, and are well described by a hyperbolic secant function.

#185319 - $15.00 USD Received 13 Feb 2013; revised 1 Apr 2013; accepted 4 Apr 2013; published 9 Apr 2013

For this proof-of-principle study, four experimental samples are considered: carbon disulfide (CS_2), pure water, 30 mM rhodamine 6G (R6G) in methanol, and pure methanol, each placed in separate glass cuvettes. Water and CS_2 are chosen because their nonlinear properties have been well studied and can be modeled using a classical approach that allows validation of the method (see section 3). In addition, water is a relevant target for biomedical applications. Methanol and R6G are chosen to directly compare the effects of two-photon absorption, since R6G has a large cross section for this type of interaction.

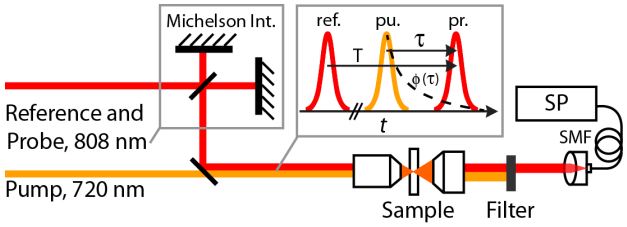

Fig. 1. The PP-NLDS system combines a pump-probe setup with a Michelson interferometer. Dotted line in inset depicts the phase dynamics of the sample induced by the pump. SP: spectrometer, SMF: single mode fiber, T: time delay between reference and probe beams, τ: time delay between pump and probe beams.

3. Theory

To understand how PP-NLDS measures wavelength-dependent intensity and phase changes from nonlinear interactions, consider a probe field that passes through a medium at the same time or after it has interacted with a pump beam (i.e., pump is 'on' with an arbitrary time-delay $\tau \geq 0$),

$$\tilde{E}_{pr}(\omega,\tau) = \tilde{E}_0(\omega)\cdot e^{-i\omega T}\cdot e^{-i(\tilde{n}_{NL}(\omega,\tau)\cdot\omega 2z_r/c)} \tag{1}$$

where $\tilde{E}_0$ is the complex reference field, z_r is the Rayleigh range of the focused beam, and $\tilde{n}_{NL}$ denotes a complex nonlinear RI resulting from any nonlinear interaction (including second or third order). Note that $\tilde{n}_{NL}$ depends on the wavelength of light, $\lambda = 2\pi c/\omega$, as well as on the time-delay between the pump and probe, τ. Further, this parameter may be expressed in terms of its real and imaginary parts, $\tilde{n}_{NL}(\omega,\tau) = n_{NL}(\omega,\tau) - ik_{NL}(\omega,\tau)$. The second term of Eq. (1) describes the time-delay between the probe and reference fields, while the third term contains all the information regarding the nonlinear interactions in the medium. Hence, when the pump is 'off,' the probe field is described by the first two terms of Eq. (1). In addition, all linear effects (attenuation and RI changes) are inherently imbedded in $\tilde{E}_0$, since the reference field follows the same path through the sample as the probe. By defining $\Phi(\omega,\tau) = -n_{NL}(\omega,\tau)\cdot\omega 2z_r/c$ and $K(\omega,\tau) = k_{NL}(\omega,\tau)\cdot\omega 2z_r/c$, the probe field may be written as,

$$\tilde{E}_{pr}(\omega,\tau) = \tilde{E}_0(\omega)\cdot e^{-K(\omega,\tau)}\cdot e^{-i(\omega T-\Phi(\omega,\tau))} \tag{2}$$

and the signal detected by the spectrometer may be expressed as,

$$\begin{aligned} I(\omega,\tau) &= \left|\tilde{E}_0(\omega)+\tilde{E}_{pr}(\omega,\tau)\right|^2 \\ &= \left|\tilde{E}_0(\omega)\right|^2 + \left|\tilde{E}_0(\omega)\right|^2\cdot e^{-2K(\omega,\tau)} + 2\left|\tilde{E}_0(\omega)\right|^2\cdot e^{-K(\omega,\tau)}\cdot\cos(\omega T+\varphi_r-\Phi(\omega,\tau)) \end{aligned} \tag{3}$$

#185319 - $15.00 USD Received 13 Feb 2013; revised 1 Apr 2013; accepted 4 Apr 2013; published 9 Apr 2013

Here, we have introduced a random variable, φ_r, to account for shot-to-shot phase variations arising from instabilities in the interferometer. The effect of φ_r will be discussed in more detail below.

The inverse Fourier transform of Eq. (3) will produce three terms, one centered at t = 0 (DC term) and two others at $t = \pm T$. If only one of the two non-DC terms is considered, then the signal (in the spectral-domain) may be described as,

$$\tilde{I}(\omega,\tau) = \left|\tilde{E}_0(\omega)\right|^2 \cdot e^{-K(\omega,\tau)} \cdot e^{-i(\omega T + \varphi_r - \Phi(\omega,\tau))} \tag{4}$$

Similarly, when the pump is 'off,' the signal is described as

$$\tilde{I}_{off}(\omega) = \left|\tilde{E}_0(\omega)\right|^2 \cdot e^{-i(\omega T + \varphi_r)} \tag{5}$$

Therefore, the nonlinear amplitude change—described by $K(\omega,\tau)$, which gives the imaginary part of $\tilde{n}_{NL}$—may be directly assessed using Eqs. (4) and (5),

$$K(\omega,\tau) = -\ln\left(\frac{\left|\tilde{I}(\omega,\tau)\right|}{\left|\tilde{I}_{off}(\omega)\right|}\right) \tag{6}$$

Pump-probe methods, however, measure the probe's transmission change due to nonlinear effects, thus we also define the fractional transmission change as,

$$\frac{\Delta\Gamma}{\Gamma} \equiv \frac{\left|\tilde{E}_{pr}(\omega,\tau)\right|^2 - \left|\tilde{E}_0(\omega)\right|^2}{\left|\tilde{E}_0(\omega)\right|^2} = \frac{\left|\tilde{I}(\omega,\tau)\right|^2 - \left|\tilde{I}_{off}(\omega)\right|^2}{\left|\tilde{I}_{off}(\omega)\right|^2} = e^{-2K(\omega,\tau)} - 1 \tag{7}$$

For small K, Eq. (7) reduces to $-2K(\omega,\tau)$.

Isolating the nonlinear phase changes, $\Phi(\omega,\tau)$, which describe the real part of the nonlinear RI, is more challenging due to the random phase term, φ_r. In the linear regime, this term is eliminated by unwrapping the phase and subtracting a straight line, which isolates the wavelength-dependent (dispersive) terms of the linear RI [20]. However $\Phi(\omega,\tau)$ may contain linear components, thus this approach would only assess second and higher order terms of $\Phi(\omega,\tau)$ with respect to ω. Here, a different approach is taken to avoid this problem, where the random phase term is eliminated by subtracting the average phase as a function of wavelength from both the 'on' and 'off' signals. This process yields Eq. (8)

$$\Phi'(\omega,\tau) \equiv \Phi(\omega,\tau) - \overline{\Phi(\tau)} = \left(\angle\tilde{I}(\omega,\tau) - \overline{\angle\tilde{I}(\tau)}\right) - \left(\angle\tilde{I}_{off}(\omega) - \overline{\angle\tilde{I}_{off}}\right) \tag{8}$$

where $\angle$ denotes the phase angle and the bar denotes the average over ω. The end parameter, $\Phi'(\omega,\tau)$, retains the spectral shape of $\Phi(\omega,\tau)$, including linear components, and significantly reduces the noise on the measured signal. Experimentally, the phase deviation (noise) per wavelength on $\Phi'(\omega,\tau)$ is two orders of magnitude lower than $\Phi(\omega,\tau)$, due to the elimination of φ_r (see section 4). This enables experimental evaluation of the small wavelength-dependent phase changes resulting from nonlinear interactions that are typically obscured by noise.

Now we describe how $\Phi(\omega,\tau)$ and $K(\omega,\tau)$ are modeled. To achieve this, it is convenient to switch from the frequency-domain to the time-domain, where the probe field may now be described as,

$$\tilde{E}_{pr}(t,\tau) = \tilde{E}_0(t-T) \cdot e^{-K(t+\tau)+i\phi(t+\tau)} \tag{9}$$

#185319 - $15.00 USD Received 13 Feb 2013; revised 1 Apr 2013; accepted 4 Apr 2013; published 9 Apr 2013

where κ and ϕ denote the time-domain intensity and phase changes, respectively, resulting from nonlinear interactions. For non-absorbing samples, the phase changes may be described using a phenomenological model of the OKE dynamics [22],

$$\phi(t) = c_1 \cdot I_{pu}(t) \otimes \left[\delta(t) + \sum_m r_m(t) \right] \tag{10}$$

Here, the first term describes the system's response, where c_1 is a proportionality constant, I_{pu} is the pump intensity, and $\otimes$ denotes a convolution. The terms in brackets represent the sample's OKE response: the delta function describes the instantaneous electronic response and the second term describes the dynamic nuclear response. For the latter, typically three terms (m = 3) are used, which describe (1) intermolecular interactions, (2) librational motion, and (3) free rotation [22]. These three terms usually take the form of single or double exponentials with a buildup response time. For the exact form used in this work for CS_2 and water, we refer the readers to refs [23] and [24], respectively [the signals are shown graphically in Fig. 2(d)]. Further, CS_2 and water do not exhibit any time-domain intensity changes, since they are non-absorbing, thus κ = 0. For samples that do exhibit intensity changes in the time-domain, more complete models that take quantum mechanics into account must be employed [25]. However, the R6G solution is subject to both resonant and dispersive effects (which have not been derived from first principles [22,23]), thus no attempts are made in this work to model the cumulative effects.

To gain some insight into the expected forms of $\Phi'(\omega,\tau)$ and $K(\omega,\tau)$, consider a non-absorbing sample with a quadratic temporal phase change, given by $\phi(t) = -\phi'' \cdot (t + \tau)^2$, which yields a simple analytical solution (see appendix). This form of the temporal phase provides a good approximation for Eq. (10) at pump-probe time-delays near the temporal phase maximum, at t = 50 fs and 165 fs for water and CS_2, respectively, as well as t = 0 for a purely electronic response. The analytical solution (detailed in the appendix) shows that the phase changes in the spectral-domain exhibit a quadratic dependence with respect to ω given by $\Phi'(\omega,\tau) \propto \phi'' \cdot (\omega - \omega_0)^2$, where ω_0 is the center frequency. Thus the concavity (up or down) of the spectral phase depends on the sign of ϕ'' or, more generally, on the second derivative of $\phi(t)$. In comparison, the transmission changes are given by $K(\omega,\tau) \propto \tau\phi'' \cdot (\omega - \omega_0)$, which has a linear dependence with respect to ω that deviates about the center frequency (i.e., no transmission change at ω_0). An intuitive way of viewing the transmission changes is that even though no intensity changes take place in the time-domain, the Fourier transform of the time-varying phase produces real and imaginary terms, where the imaginary term will manifest itself as spectral intensity changes. In addition, the spectrum must be an odd function about ω_0, to ensure that the net effect disappears in the conjugate domain. It is also worth noting that the slope of $K(\omega)$ at a given time-delay, τ, changes signs when the temporal phase, $\phi(t)$, reaches a maximum ($\phi(\tau = 0)$ in this case).

As a last theoretical note, it is important to understand that the pump induces a time-dependent polarization change on the medium that precedes the probe field; as a result, the causality conditions between the probe field and the induced polarization are no longer fulfilled [25,26]. Consequently, the real and imaginary parts of the polarization (and hence nonlinear complex refractive index) are, in general, not related via the Kramers-Kroning relations. This is significant for the present work because it implies that both measured parameters, Φ and K, contain 'new' information regarding the nonlinear response of the medium.

#185319 - $15.00 USD Received 13 Feb 2013; revised 1 Apr 2013; accepted 4 Apr 2013; published 9 Apr 2013

4. Results and discussion

A representative raw signal (from water and $\tau = 0$) is shown in Fig. 2(a). As described in section 3, this signal is Fourier transformed and filtered in the time-domain to isolate the interferometric term. This has the added benefit of removing any other signals that may be produced from reflections along the beams' path. Here, a 10th order Butterworth filter is used. The signal is then transformed back to the frequency-domain, which yields the complex field as described by Eqs. (4) and (5). Figures 2(b) and 2(c) illustrate this process.

After processing both the 'on' and 'off' signals, the amplitude and phase changes resulting from nonlinear interactions can be ascertained using Eqs. (7) and (8), respectively. To avoid high noise levels in the experimental signals, we only consider a spectral region where the amplitude of $\left|\tilde{I}(\omega)\right|$ is above 0.4 (as was done in [20,21]). For the theoretical simulations, the fields are first defined in the time-domain and then Fourier transformed to give the fields in the frequency-domain [which gives Eq. (1)]. The theoretical results, given by Eqs. (7) and (8), can be determined directly from the simulated complex field in the frequency-domain. Further, the proportionality constant c_1 in Eq. (10) is adjusted to qualitatively match the amplitude of the experimental phase changes—we find that values of 0.02 and 0.035 provide good agreement for water and CS_2, respectively. The modeled OKE responses [Eq. (10)] are illustrated in Fig. 2(d). Figures 3-4 show the experimental results of 10 independent measurements from water and CS_2 along with the theoretical simulated signals.

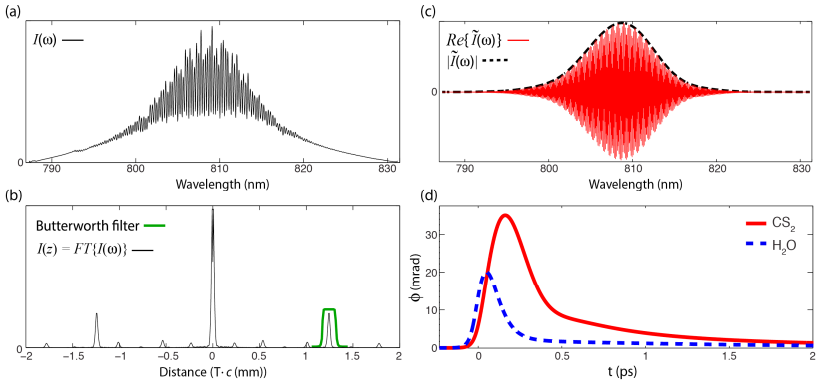

Fig. 2. Processing method for PP-NLDS. The raw signal measured by the spectrometer (a) is Fourier transformed and filtered in the time-domain to isolate the interferometric term (b). The signal is then transformed back to the frequency-domain to gain access to the complex form of the field (c). (d) Simulated OKE response for water and CS_2 [23,24].

The experimental results and the theoretical simulations at $\tau = 0$ for Φ' (solid red curves in Figs. 3-4) are in excellent agreement, where both show the same concavity (up or down) and slight asymmetry in the parabolic shape for each sample. These results can be understood by using the approximation provided in section 3 (and appendix): Specifically, the difference in concavity between the two samples results from the fact that the OKE response of CS_2 peaks at a later time compared to water, which causes the second derivatives to have opposite signs at $\tau = 0$. These are drastic changes that reflect important features of the OKE response, and highlights how Φ' can readily reveal the diffusive motions of molecules. We also note that the average standard deviation of Φ' per wavelength (spectral phase noise) is ~0.1 mrads. In comparison, the spectral phase noise of Φ, which does not take the random phase term (φ_r) into account, is ~20 mrads, and thus this parameter significantly obscures the spectral features of interest. This result underscores the importance of accounting for the random phase noise term using the spectral information [as described by Eq. (8)]. Figure 3(c) shows Φ for CS_2, where the influence of φ_r is clearly visible.

#185319 - $15.00 USD Received 13 Feb 2013; revised 1 Apr 2013; accepted 4 Apr 2013; published 9 Apr 2013

The transmission changes as a function of wavelength also show relatively good agreement, though a small discrepancy is observed for the water sample. Nevertheless, the important features here are that (1) the spectra are approximately linear, with zero transmission change at the center wavelength, in good agreement with the analytical analysis; and (2) matching the amplitude of the phase between the experiment and simulation using the constant c_1 in Eq. (10), also provides good agreement between the amplitude of the transmission changes (i.e., both experiment and simulation span a range of ~ ± 1%). The discrepancy in the slope of the water transmission spectrum at $\tau = 0$ can be attributed to error in the pump-probe time delay. For example, according to our OKE model for water [24], the maximum temporal phase change occurs at ~50 fs, at which point, the slope of the transmission spectrum will change from positive to negative. Such small pump-probe time-delay error in the experiment is not unreasonable considering that the cross-correlation of the pump and probe, used to find $\tau = 0$, has a FWHM of ~200 fs (shift of +/– 100 fs are within experimental error). Figure 4(c) illustrates the theoretical transmission and phase changes modeled at a time-delay $\tau = 75$ fs. The simulation displays transmission changes with a negative slope and phase changes with negative concavity, in excellent agreement with the experimental measurements.

The transmission data also show that the signal-to-noise ratio (noise is ~1% averaged over wavelength) is worse than that of the phase spectrum. This is not surprising because the transmission noise cannot be eliminated in the same way as the phase noise, since we are generally interested in transmission offsets. In addition, absorption measurements in the linear regime using NLDS have shown that the amplitude of the field is two orders of magnitude less sensitive compared the phase [21]. To reduce the noise in the transmission signal in the nonlinear regime, further development of the experimental setup is needed; for example, modulating the pump and using lock-in-detection would significantly reduce the low frequency noise of the source, which is likely the main contributing factor here (see section 5: conclusion and future work).

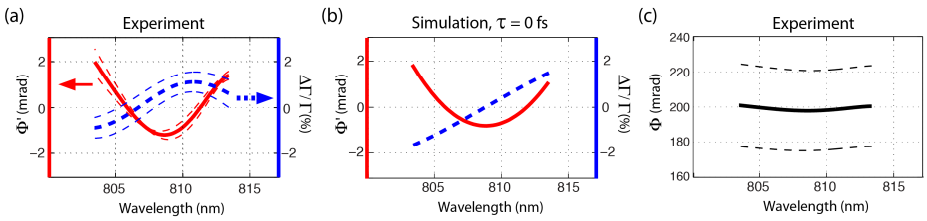

Fig. 3. Experiment (a) and numerical simulations at $\tau = 0$ fs (b) for CS_2. The experiment and simulated signals are in excellent agreement. (c) Spectral phase Φ, which does not account for the random phase term, φ_r. Thin dashed lines represent the standard deviation of 10 measurements.

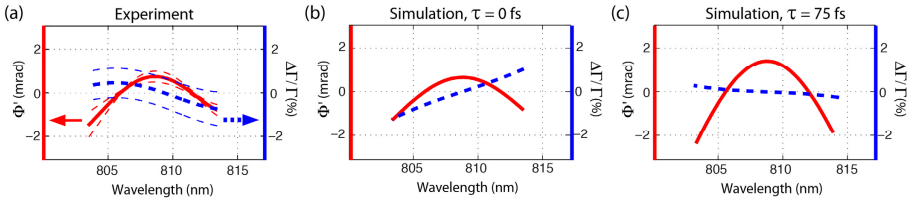

Fig. 4. Experiment (a) and numerical simulations at $\tau = 0$ fs (b) and $\tau = 75$ fs (c) for water. A discrepancy is observed in the transmission signal of water at $\tau = 0$. This can be rectified by considering small errors in the setup that may shift τ to different values (shift of +/– 100 fs are within experimental error, limited by the cross correlation of the pump and probe pulses ~200 fs). A simulated signal at $\tau = 75$ fs provides excellent agreement (c). Thin dashed lines represent the standard deviation of 10 measurements.

#185319 - $15.00 USD Received 13 Feb 2013; revised 1 Apr 2013; accepted 4 Apr 2013; published 9 Apr 2013

To better understand these results, we compare theoretical simulations of the phase and transmission changes as a function of wavelength and time-delay between the pump and probe, τ, for pure water, CS_2 and an instantaneous electronic response [delta term in Eq. (10)]. The results are shown in Fig. 5, where in general the phase behavior shows a parabolic shape as a function of wavelength, and the transmission changes show a linear dependence. Moreover, the concavity (up or down) of the spectral phase corresponds to the sign of the second derivative of the temporal OKE response, thus the points of inflection give an indication of the time when the spectral phase changes concavity. Similarly, these inflection points correspond to when the slope of the spectral-transmission-changes reach a maximum, which is in good agreement with spectral shifting methods [8]. The time when the spectral transmission changes go to zero (and thus when the transmission slope changes signs) resembles the time when the OKE response is at a maximum (i.e., first derivative is zero). It is important to note that the instantaneous electronic response, shown in Figs. 5(c) and 5(f), produces spectral phase and transmission dynamics that are symmetrical about $\tau = 0$, unlike water and CS_2, also shown in Fig. 5. The nuclear repose of OKE causes this imbalance. Thus, the rich structure of the spectral phase and transmission changes offer a wealth of information that provides molecular contrast of non-pigmented samples.

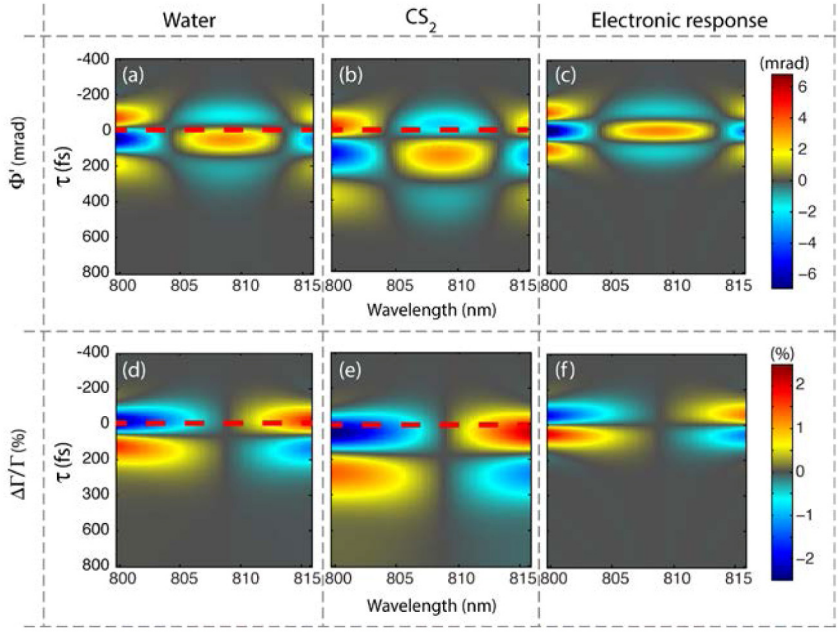

Fig. 5. Simulated nonlinear response of water, CS_2 and an instantaneous electronic response [delta term in Eq. (10)] as a function of wavelength and time-delay between pump and probe, τ. Red dashed lines are located at $\tau = 0$, corresponding to the delay of the experimental/simulated results shown in Figs. 3 and 4.

Lastly, we investigate the effects of two-photon absorption (a resonant interaction) by comparing methanol and R6G (in methanol), which contains a large two-photon cross section. Figure 6(a) shows that both samples have similar spectral phase dependence, which is not unexpected considering that both samples contain methanol. However, the transmission spectra [Fig. 6(b)] show important differences, where R6G exhibits a loss in transmission at all wavelengths, which captures the effects of two photon absorption. For pure methanol, the transmission spectrum deviates about zero, as with the other non-absorbing samples. The loss in transmission for R6G is also clearly observed in the in the time-domain [Fig. 6(c)]—this illustrate how PP-OCT draws its molecular contrast.

#185319 - $15.00 USD Received 13 Feb 2013; revised 1 Apr 2013; accepted 4 Apr 2013; published 9 Apr 2013

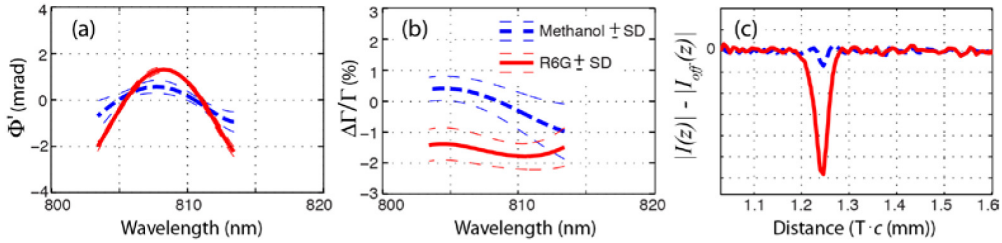

Fig. 6. Experimentally measured nonlinear optical response of methanol and R6G. Phase (a) and transmission (b) changes as a function of wavelength, and transmission changes in the time-domain (c).

5. Conclusion and future work

The experimental results presented here demonstrate that PP-NLDS can ascertain a sample's dispersive and resonant (real and imaginary, respectively) nonlinear optical response to a pump beam. The theoretical framework for non-resonant samples provides a relatively simple explanation of the observed behavior that is in good agreement with the experimental measurements. An important feature of this method is its ability to gain access to small nonlinear spectral-phase changes, which is only possible when the random phase noise is accounted for. The resulting dynamics accentuate important features of the OKE response, and offer a wealth of information for molecular contrast. The method is also sensitive to resonant effects, and can therefore obtain the same information as conventional pump-probe methods, with added information from two other dimensions (wavelength and phase).

Future work will focus on further developing the system for imaging biological samples. Specifically, the pump beam will be placed on a variable time delay stage, which will grant experimental access to the fourth dimension, τ, and should help mitigate setup errors. Backscattering geometries will also be explored to enable in-vivo applications. Finally, the pump beam will be modulated to reduce low frequency noise from the source. This is expected to provide better SNR, in addition to potentially enabling assessment of the average phase as a function of time-delay (i.e., $\Phi(\omega,\tau)$ instead of $\Phi'(\omega,\tau)$).

In conclusion, we expect that the ability to sample four dimensions (phase, amplitude, wavelength, and pump-probe time delay) will enable extremely specific and sensitive contrast for a wide range of molecules for biomedical imaging.

Appendix

In this section we derive an analytical expression for the phase and amplitude, frequency-dependent changes on an optical field that result from nonlinear interactions with a non-absorbing sample. First, consider the unperturbed field in the time-domain with a Gaussian envelope:

$$\tilde{E}_0(t) = e^{-at^2} \cdot e^{i\omega_0 t} \tag{11}$$

where a describes the width of the Gaussian pulse and ω_0 is the center frequency. In the frequency domain the field is described as,

$$\begin{aligned} \tilde{E}_0(\omega) &= \int_{-\infty}^{\infty} e^{-at^2} \cdot e^{-i(\omega-\omega_0)t}\, dt \\ &= \frac{1}{\sqrt{2a}} \cdot \exp\left(-\Omega^2/(4a)\right) \end{aligned} \tag{12}$$

#185319 - $15.00 USD Received 13 Feb 2013; revised 1 Apr 2013; accepted 4 Apr 2013; published 9 Apr 2013

with $\Omega = \omega - \omega_0$. When the pump beam interacts with the sample, the pump introduces a transient perturbation on the refractive index of the sample via the optical Kerr effect, $n = n_0 + \delta n$. As the probe field propagates through the perturbation, it acquires a time-dependent phase modulation, which may be express as a Tyler series,

$$\phi(t) = \phi_0 + \phi' t + \phi'' t^2 + \ldots \tag{13}$$

where the primes denote a derivative with respect to time, t (constants are ignored for simplicity). Because the method described in this work is insensitive to phase offsets, ϕ_0 can be ignored. Further, if we consider the electronic response near time delays when the pump and probe are temporally overlapped, then $\phi' \sim 0$ since the response can be well represented by a second order function. Higher order terms are assumed to be negligible. The resulting temporal phase change experienced by the probe field is described by,

$$\phi(t) = -\phi'' \cdot (t + \tau)^2 \tag{14}$$

where ϕ'' is a positive constant that depends on the sample. Note that we have explicitly accounted for the pump-probe time delay, τ. This form of the temporal phase provides a good approximation for Eq. (10) at pump-probe time-delays near the temporal phase maximum at t = 50 fs and 165 fs for water and CS_2, respectively, as well as t = 0 for a purely electronic response. Following Eq. (9), the field in the Fourier domain is now given by,

$$\tilde{E}_{pr}(\omega) = \int_{-\infty}^{\infty} e^{-at^2} \cdot e^{i\phi'' \cdot (t+\tau)^2} \cdot e^{-i(\omega - \omega_0)t}\, dt \tag{15}$$

$$= \frac{1}{\sqrt{2a - i\,2\phi''}} \cdot \exp\left(\frac{ia\phi''\tau^2 + \phi''\tau\Omega - \Omega^2/4}{a - i\,\phi''} \right) \tag{16}$$

To separate the real and imaginary parts, we multiply the terms in the exponential by the complex conjugate of the denominator, which yields:

$$-\frac{(\Omega/2 - \phi''\tau)^2}{a} - i\,\phi'' \cdot \frac{(\Omega/2 - \phi''\tau)^2 - \tau^2 \cdot (\phi''^2 - a^2)}{a^2} \tag{17}$$

Therefore, Eq. (16) can be expressed as,

$$\tilde{E}_{pr}(\Omega) = \tilde{C}_0 \cdot e^{-\frac{(\Omega/2 - \phi''\tau)^2}{a}} \cdot e^{-i\phi'' \cdot \frac{(\Omega/2 - \phi''\tau)^2}{a^2}} \tag{18}$$

where $\tilde{C}_0$ is a complex constant. Equation (18) gives the familiar form of a spectral shift, as previously described in Ref [8], along with a quadratic phase change with respect to frequency. Equation (18) can be further simplified to yield a solution of the resulting probe field that fits the form of Eq. (2). In other words, we want to write the resulting field as the original unperturbed field multiplied by an absorptive and dispersive term. By expanding the exponentials and only retaining the largest terms (with $\Omega^2/4 >> \Omega\phi''\tau >> (\phi''\tau)^2$, since ϕ'' and τ are small constants) we finally obtain,

$$\tilde{E}_{pr}(\Omega) \approx \tilde{C}\tilde{E}_0 \cdot e^{\phi''\tau\Omega/a} \cdot e^{-i\,\phi'' \cdot (\Omega/2a)^2} \tag{19}$$

Here $\tilde{C}$ is a different complex constant that accounts for all the frequency-independent terms. The analytical solution shows a quadratic phase dependence with respect to frequency, and an

#185319 - $15.00 USD Received 13 Feb 2013; revised 1 Apr 2013; accepted 4 Apr 2013; published 9 Apr 2013

exponential response that varies linearly with frequency. Note that the slope of the spectral transmission also depends on τ, which means that when the pump beam is temporally overlapped with the probe ($\tau = 0$) the amplitude is unmodulated. This is in agreement with the experiments and numerical simulations shown in Figs. 3-5. This analytical treatment gives an accurate description of the frequency-dependent phase and amplitude changes observed for non-absorbing samples.

Acknowledgments

We thank the Wax group for providing the high-resolution spectrometer. This work was supported by the National Institutes of Health grants 1RC1CA145105 and R01-CA166555, and Duke University.

#185319 - $15.00 USD Received 13 Feb 2013; revised 1 Apr 2013; accepted 4 Apr 2013; published 9 Apr 2013